Multi-angle aerosol optical depth retrieval method based on improved surface reflectance

Lijuan Chen[1], Ren Wang[1], Ying Fei[2], Peng Fang[2],Yong Zha[2], Haishan Chen[1*]

[1]Key Laboratory of Meteorological Disaster, Ministry of Education (KLME)/Joint International Research Laboratory of Climate and Environment Change (ILCEC)/Collaborative Innovation Center on Forecast and Evaluation of Meteorological Disasters (CIC-FEMD), Nanjing University of Information Science and Technology, Nanjing 210044, China

[2]Key Laboratory of Virtual Geographic Environment of Ministry of Education, Jiangsu Center for Collaborative Innovation in Geographical Information Resource Development and Application, College of Geographic Science, Nanjing Normal University, Nanjing 210023, China

Correspondence: Haishan Chen (haishan@nuist.edu.cn)

Abstract

Retrieval of atmospheric aerosol optical depth (AOD) has been a challenge for Earth satellite observations, mainly due to the difficulty in estimating surface reflectance with the combined influence of land-atmosphere coupling. Current major satellite AOD retrieval products have low spatial resolution under complex surface processes. In this study, we further improved the surface reflectance by modeling the error correction based on the previous AOD retrieval and obtained more accurate AOD retrieval results. A lookup table was constructed using the Second Simulation of Satellite Signal in the Solar Spectrum (6S) to enable high-precision AOD retrieval. The accuracy of the algorithm's retrieval was verified by the Aerosol Robotic Network observations (AERONET). From the validation results, we find that among the nine Multi-angle Imaging

SpectroRadiometer (MISR) angles, the retrieved AOD has the best retrieved results with the AOD observed at the An angle (Taihu: R=0.81, RMB=0.68; Xuzhou-CUMT: R=0.73, RMB=0.78). This study will help to further improve the retrieval accuracy of multi-angle AOD at large spatial scales and long time series. The retrieved AOD based on the improved method has the advantages of fewer missing pixels and finer spatial resolution compared to the MODIS AOD products and our previous estimates.

Keywords: surface reflectance; aerosol optical depth; satellite remote sensing; MISR; MODIS

1. Introduction

Aerosols are liquid or solid particles suspended in the atmosphere, with particle diameters ranging from approximately 0.001 to 100 μm (Giles et al., 2019). Aerosol particles suspended in the atmosphere not only affect the radiative forcing of the Earth's air system through direct, indirect or semi-direct action, but also influence climate, and cause environmental problems such as acid rain and haze (Hatzianastassiou et al., 2009; Dao et al., 2014; Daniel et al., 2014; Samset et al., 2018; Li et al., 2018; Huang et al., 2021). Therefore, the study of aerosol distribution and change trend has become a hot topic in the field of aerosol research (Holben et al., 2001; Li et al., 2020; Berhane et al., 2021; Sun et al., 2022). In addition, high concentrations of aerosols can pose a serious threat to human health (Lee et al., 2010; Dehghani et al., 2012; Mironova et al., 2015). The optical properties of aerosols include parameters such as aerosol optical depth (AOD), scattering phase function, single scattering albedo, and absorbing optical depth. Among them, AOD is an important parameter defined as the integral of the aerosol extinction coefficient in the vertical direction. It describes the attenuation effect of aerosols on light and is an important indicator of the level of air pollution. Multi-channel spectrometers on board geostationary and

polar orbiting satellites have been used for AOD retrieval in the last two decades. The AOD products obtained through satellite retrievals are widely used in atmospheric environmental studies (Kaufman et al, 1997; Xie et al., 2019; Chen et al., 2021). Although the accuracy of AOD retrieval has been improving, there is still much room for improvement in the AOD retrieval on land when more complex influences are taken into account.

Scholars have conducted research on AOD retrieval using satellite-based multi-angle sensors. Kokhanovsky et al. (2009) used the Along-Track Scanning Radiometer Dual View (ATSR-DV) algorithm to retrieve AOD over Germany and compared the retrieval results with the Medium Resolution Imaging Spectrometer (MERIS) and Multi-angle Imaging SpectroRadiometer (MISR) products. The results show that the ATSR-2 algorithm is also applicable to the Advanced Along-Track Scanning Radiometer (AATSR). Sundstrom et al. (2012) obtained an aerosol model of eastern China based on Aerosol Robotic Network (AERONET) observation data and used the ATSR-DV algorithm to retrieve the proportion of AOD and coarse to fine particles from AATSR data. Abdou et al. (2005) compared the MISR AOD and the Moderate-resolution Imaging Spectroradiometer (MODIS) AOD products carried by Terra using data from 62 AERONET observation sites. The results show that over land, the MODIS AOD of 0.470 um and 0.660 um channels is 35% and 10% higher than that of MISR, respectively. In coastal and desert areas, MODIS retrieval error is large, while over the ocean, at 0.470 um and 0.660 um channels, MISR is 0.1 and 0.05 higher than MODIS AOD value, mainly depending on the accuracy of radiometric calibration. Martochik et al. (1997) proposed an algorithm for extracting aerosol optical parameters using MISR multi-angle observations. The results show that the low reflectance of vegetation and multi-angle observation data are used to retrieve AOD in the case of dense land

vegetation. As a new remote sensing tool, multi-angle remote sensing can provide aerosol optical depth, single scattering albedo, phase function and other features with sufficient accuracy, which is more suitable for playing its unique role in aerosol research than traditional single-angle optical remote sensing (Dubovik et al., 2019). Multi-angle remote sensing retrieval of aerosol optical properties can use the angle information contained in satellite signals to better separate the contributions of the surface and atmosphere, which is suitable for some bright surfaces. This provides a new way for AOD retrieval.

Surface reflectance measures the ability of land to absorb and reflect solar radiation. On land, surface reflectance is relatively complex and is detected by satellite sensors after atmospheric scattering and absorption. Satellite observations capture the combination of there two components, making it challenging to directly separate surface reflectance from atmospheric scattering. Therefore, simultaneous acquisition of atmospheric aerosols and surface reflectance is the main objective of quantitative satellite remote sensing (Deuzé et al., 2001). In optical remote sensing, the blue wavelength is shorter and the surface reflectance is lower, resulting in more atmospheric reflection and scatteringm. Blue band is commonly used for AOD retrieval. In the process of AOD retrieval, overestimation of surface reflectance leads to underestimation of AOD, while underestimation of surface reflectance leads to overestimation of AOD. In general, aerosol signals are weaker than surface signals (Dong et al., 2023). Previous studies have shown that when the surface reflectance intercept error is 0.01, the error of satellite remote sensing retrieval AOD is about 0.1 (Zhang et al., 2021). Therefore, accurate estimation of surface reflectance is very importance for the accurate retrieval of aerosol optical depth.

In order to improve the accuracy and resolution of MISR AOD retrieval, we analyzed the

MISR AOD retrieval errors of 9 camera angles in previous studies. Secondly, by establishing an error correction model, we modify the surface reflectance of MISR to improve the accuracy of surface reflectance estimation. Finally, the improved AOD is verified with the ground observation site AOD data, and the retrieval results are compared with the previous retrieval results and MODIS AOD products.

2. MISR, MODIS, and AERONET Data

2.1 MISR data

In this study, we employed MISR Level 1B2 terrain data (MI1B2T) and used HEGTool (HDF-EOS To GeoTIFF Conversion Tool) software to extract radiation data. Blocks 64 and 65 covering the Yangtze River Delta region were extracted by selecting corresponding blocks, output data types and projections based on the regional locations of 180 blocks (Figure S1). In addition, we extracted the solar zenith angle, solar azimuth angle, satellite zenith angle, and satellite azimuth angle data of 9 cameras from the angle dataset (MI1B2GEOP) and selected the corresponding blocks, output data types and projection information. To reduce the influence of cloud, we carried out cloud detection and cloud pixel removal on satellite remote sensing images with cloud pixel coverage less than 50%, and used blue band threshold to remove cloud pixels. However, through repeated experiments, we found that the fixed threshold was not effective in removing cloud pixels at 9 angles of the MISR sensor (Figures S2 and S3). Therefore, we use dynamic threshold method to remove cloud pixels from MISR data. Details of the data used in this study are shown in Table S2.

2.2 MODIS data

In this study, we used MODIS L1B data, including radiance data (MOD02/MYD02) and geolocation data (MOD03/MYD03). Data preprocessing using the MODIS Conversion Toolkit (MCTK) tool, including radiation calibration, butterfly processing, geometric correction, reprojection, and band extraction. MODIS BRDF/Albedo is a standard Level 3 product that represents the surface characteristics of MODIS instruments on the Terra and Aqua satellite platforms. The product retrieval cycle is 16 days, and the observations on day 9 of each 16-day cycle are weighted to generate daily data, called the global daily surface albedo product (Hsu et al., 2004). The core data set for the MODIS BRDF product is MCD43A1.

2.3 AERONET data

AERONET uses the CE-318 instrument, a solar radiation photometer produced in France, which obtains direct solar spectral radiation measurements at 340, 380, 440, 500, 670, 870, 936, 1020 and 1640 nm channels at 1.5° field angles every 3 min. The total water vapor content of the atmosphere can be obtained in the 936 nm channel. The AOD value can be retrieved by the measured value of other channels, and the retrieval error is about 0.01-0.02. Therefore, it can provide aerosol characteristic parameters with high accuracy and verify aerosol parameters retrieved by satellite (Lu et al., 2019). In this study, AERONET AOD values are used as truth values to verify the accuracy of satellite remote sensing AOD retrieval. AERONET AOD data is classified into three levels: Level 1.0 (unfiltered), level 1.5 (cloud screening and quality control) and level 2.0 (quality assurance). The study area mainly covers the Yangtze River Delta, and there are several ground observation sites in the area. However, only two observation sites, Taihu and

Xuzhou-CUMT sites have continuous observation data, while the duration of other sites is relatively limited. Therefore, AERONET Level 1.5 AOD data with a large number of observed values were selected to verify the retrieval results of MISR AOD.

3. Methodology

3.1 Problems in the previous surface reflectance estimation method

Accurate estimation of surface reflectance is a crucial and challenging aspect in the retrieval of AOD from satellite remote sensing data (Remer et al., 2009; Gupta et al., 2016). Previous research has identified the variation patterns of 9-angle MISR AOD (Chen et al., 2021). However, the AOD retrieved from 9 angles shows relatively large errors compared to AERONET AOD (Table S3). Atmospheric correction can eliminate the effects of clouds and aerosols and obtain true surface reflectance. The reflectance of MISR is calculated by inputting geometric parameters, AOD, aerosol type, sensor radiation brightness data and sensor height into 6S model. In this study, we input MISR geometric parameters and radiation data corresponding to Taihu and Xuzhou-CUMT sites, and AOD parameters are AERONET AOD values of these two sites. The reflectance of atmospheric correction for each pixel is calculated by the linear atmospheric correction formula. To explore the reasons for the high AOD value of the retrieval from 9 MISR angles, the MISR atmospheric correction reflectance and MISR surface reflectance were compared at the corresponding locations of the two sites (Figure 1) (MISR surface reflectance calculation method referenced Chen et al. (2021)). The results show that the surface reflectance of MISR is lower than the atmospheric reflectance of MISR. The MISR AOD retrieved is higher compared to the AERONET AOD. Therefore, it is necessary to establish a correction model to

improve the MISR surface reflectance and improve the retrieval accuracy of MISR AOD.

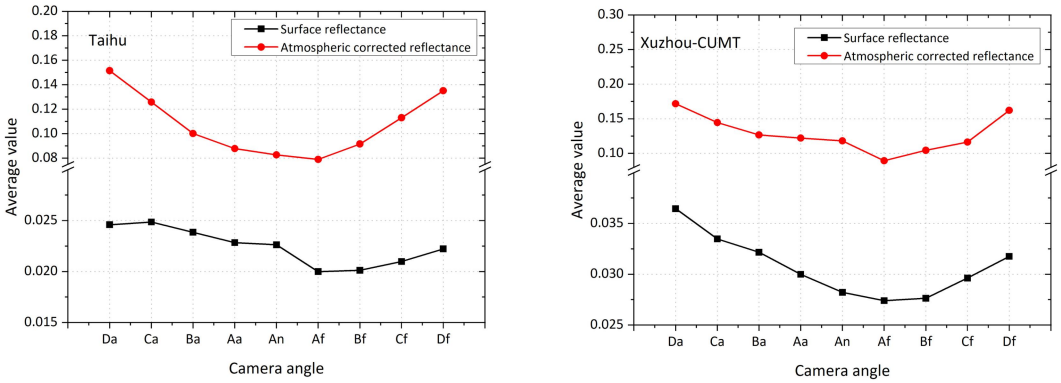

Figure 1. Comparison of MISR surface reflectance and atmospheric corrected reflectance in blue band (At the pixel locations of Taihu and Xuzhou-CUMT sites).

3.2 Improved surface reflectance estimation method

To construct an improved surface reflectivity correction model, the specific steps are shown as follows:

(1) Calculation of MODIS atmospheric corrected reflectance

The MODIS L1B data is corrected by the 6S model, and the MODIS atmospheric correction reflectance is obtained. When using 6S model to calculate MODIS atmospheric correction reflectivity, it is necessary to provide geometric parameters, AOD, atmospheric mode, aerosol type, sensor radiance data, sensor height, spectral parameters and other parameters. In this study, MODIS geometric parameters and radiance data corresponding to Taihu and Xuzhou-CUMT sites are used. The AOD parameters were obtained from AERONET AOD data at both sites. Atmospheric models select mid-latitude winter and mid-latitude summer to account for seasonal variations in atmospheric transport. The aerosol type selected in this study is continental aerosol. The sensor height is set to the observation height of the satellite. The spectral parameters are

defined according to the band of the MODIS sensor. By providing these parameters, we can calculate the atmospheric correction reflectance of the MODIS sensor using the 6S model.

(2) Surface bidirectional reflectance Calculation

MODIS BRDF/Albedo product MCD43A1 data and Ross-Li model were used to simulate surface bidirectional reflectance under MODIS and MISR observation geometry. The linear kernel driven BRDF model includes three basic parameters: the reflectance of the lowest point view and the weighting coefficient of the two kernel functions. The model can be calculated using formulas 1-9.

$$BRDF(\theta_s,\theta_v,\phi) = f_{iso}(\Lambda) + f_{vol}(\Lambda)K_{vol}(\theta_s,\theta_v,\phi) + f_{geo}(\Lambda)K_{geo}(\theta_s,\theta_v,\phi) \quad (1)$$

$$K_{vol}(\theta_s,\theta_v,\phi) = \frac{(\pi/2-\xi)\cos\xi + \sin\xi}{\cos\theta_s + \cos\theta_v} - \frac{\pi}{4} \quad (2)$$

$$K_{geo}(\theta_s,\theta_v,\phi) = O(\theta_s,\theta_v,\phi) - \sec\theta'_s - \sec\theta'_v + \frac{1}{2}(1+\cos\xi')\sec\theta'_s\sec\theta'_v \quad (3)$$

$$O(\theta_s,\theta_v,\phi) = \frac{1}{\pi}(t-\sin t\cos t)(\sec\theta'_s + \sec\theta'_v) \quad (4)$$

$$\cos t = \frac{h}{b}\frac{\sqrt{D^2+(\tan\theta'_s\tan\theta'_v\sin\phi)^2}}{\sec\theta'_s+\sec\theta'_v} \quad (5)$$

$$D = \sqrt{\tan^2\theta'_s + \tan^2\theta'_v - 2\tan\theta'_s\tan\theta'_v\cos\phi} \quad (6)$$

$$\cos\xi' = \cos\theta'_s\cos\theta'_v + \sin\theta'_s\sin\theta'_v\cos\phi \quad (7)$$

$$\theta'_s = \tan^{-1}(\frac{b}{r}\tan\theta_s) \quad (8)$$

$$\theta'_v = \tan^{-1}(\frac{b}{r}\tan\theta_v) \quad (9)$$

In the above equations, $BRDF(\theta_s,\theta_v,\phi)$ is the surface bidirectional reflectance, while θ_s, θ_v, and ϕ are the solar zenith angle, the satellite zenith angle, and relative azimuth angle, respectively. Λ is bandwidth, while $K_{vol}(\theta_s,\theta_v,\phi)$ and $K_{geo}(\theta_s,\theta_v,\phi)$ are volumetric scattering kernel and geometric optical scattering kernel, respectively, which are functions of the angle of

incidence and the angle of observation. f_{iso}, f_{vol}, and f_{geo} are the weights assigned to isotropic scattering, volumetric scattering, and geometric optical scattering, respectively. ξ is the scattering angle, while *b*, *h*, and *r* represent vertical radius of the sphere, horizontal radius of the sphere and height of the center of the sphere, respectively. These three parameters can be defined as fixed values. In the production process of the MODIS BRDF model, the relationship between *h*, *b* and *r* parameters is h/b=2 and b/r=1 (Schaaf et al., 1999). According to the above equation, the surface bidirectional reflection under any incident direction of the sun and observation direction of the satellite can be obtained by extrapolating the nucleus.

(3) Improved MISR surface reflectance calculation

The MODIS atmospheric correction reflectance is brought into Eq. 10 and Eq. 11, and a new MISR surface reflectance estimate based on MODIS atmospheric correction is calculated. Regression fitting of MISR surface reflectance with the newly estimated MISR surface reflectance was performed (60% of the total sample data was randomly selected), and the surface reflectance error correction model was finally established, as shown in the following equation:

$$\rho(\theta_s,\theta_v,\phi)_{MISR\_a} = \rho(\theta_s,\theta_v,\phi)_{MODIS\_at} \times \frac{BRDF(\theta_s,\theta_v,\phi)_{MISR}}{BRDF(\theta_s,\theta_v,\phi)_{MODIS}} \quad (10)$$

In Eq. 10, $BRDF(\theta_s,\theta_v,\phi)_{MISR}$ and $BRDF(\theta_s,\theta_v,\phi)_{MODIS}$ are BRDFs obtained under MISR and MODIS angles, respectively. θ_s is the solar zenith angle, θ_v is the satellite zenith angle, and ϕ is the relative azimuth angle. $\rho(\theta_s,\theta_v,\phi)_{MISR\_a}$ is the surface reflectance of MODIS at the geometric observation angle of MISR, and $\rho(\theta_s,\theta_v,\phi)_{MODIS\_at}$ is the MODIS atmospheric corrected reflectance.

In this study, spectral data containing the typical characteristics of 28 different types of

vegetation, soil and water bodies were selected from 5 standard spectral libraries included with ENVI software. The surface reflectance of MODIS and MISR sensors in the blue band is calculated by the formula (Chen et al., 2021).

$$\rho(\theta_s,\theta_v,\phi)_{MISR} = \rho(\theta_s,\theta_v,\phi)_{MISR\_a} \times 0.9834 - 0.0081 \quad (11)$$

The New MODIS surface reflectance ($\rho(\theta_s,\theta_v,\phi)_{MISR\_a}$) at the MISR angle obtained from Eq. 10 is converted to the MISR surface reflectance by Eq. 11.

The MISR surface reflectance estimated by Eq. 11 was transformed using an error correction model to obtain an improved MISR surface reflectance. The improved MISR surface reflectance will be used for AOD retrieval. The MISR surface reflectance previously estimated based on MODIS V5.2 algorithm was fitted with the MISR surface reflectance estimated based on MODIS atmospheric correction (60% of the data were randomly selected) by linear regression, and a MISR correction model was established, as shown in Eq. 12. The previously estimated 9-angle MISR surface reflectance is corrected by Eq. 12, and the improved surface reflectance of the MISR sensor at 9 angles is obtained, and finally used for MISR AOD retrieval at 9 angles.

$$\rho(\theta_s,\theta_v,\phi)_{MISR-b}{}^{*} = \rho(\theta_s,\theta_v,\phi)_{MISR} \times 0.9209 + 0.0409 \quad (12)$$

Where $\rho_{MISR-b}{}^{*}$ is the improved MISR surface reflectance in Eq. 12.

3.3 Flow of improved multi-angle AOD retrieval

The flow of the improved surface reflectance algorithm in this study is shown in Figure 2. Firstly, the atmospheric correction of MODIS L1B data is performed using 6S model. Then, the MISR surface reflectance estimated by previous study was combined with the new MISR surface reflectance estimated by Eq. 11 to build a MISR error correction model for obtaining the improved

MISR surface reflectance (Chen et al., 2021). The study retrieved the MISR AOD for nine camera angles using improved MISR surface reflectance. We validated the improved MISR AOD with AERONET AOD. We compared the improved AOD with the previously retrieved AOD and analyzed the accuracy and spatial distribution trends of the improved AOD. The AOD retrieval method used in this study is based on chen et al. (2021). In our study, we used continental aerosols for AOD retrieval and 6S model for atmospheric correction. Choosing the right aerosol type is crucial for obtaining accurate aerosol optical depth. Previous studies have shown that continental aerosols can be used to estimate aerosol optical depth in the Yangtze River Delta (He et al., 2015). In this study, the same aerosol type was used for AOD retrieval and atmospheric correction, and the error transfer caused by aerosol type and atmospheric correction was not considered.

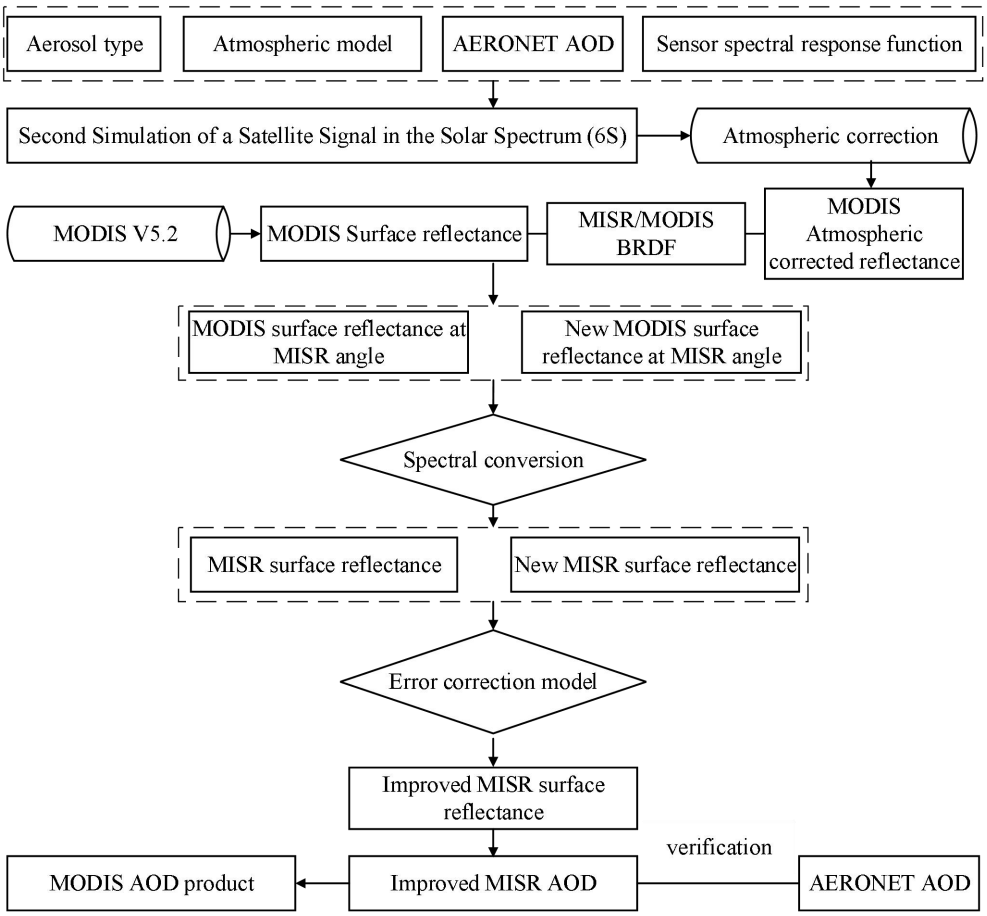

Figure 2. Flow chart of the improved MISR surface reflectance algorithm

4. Results and discussion

4.1 Improved MISR surface reflectance variation characteristics

The variation characteristics of MISR surface reflectance, MISR atmospheric correction reflectance and improved MISR surface reflectance are shown in Figure 3. These values are the average values of all sample data collected at the corresponding locations of the two sites in Taihu and Xuzhou-CUMT during the period of validity from 2016-2018. At Taihu and Xuzhou-CUMT sites, the improved MISR surface reflectance of 9 camera angles is generally higher than that of MISR surface reflectance, and lower than that of MISR atmospheric correction reflectance. The surface reflectance of 9 camera angles MISR is between 0.02 and 0.04. On average, the improved surface reflectance is higher than the previously estimated MISR surface reflectance.

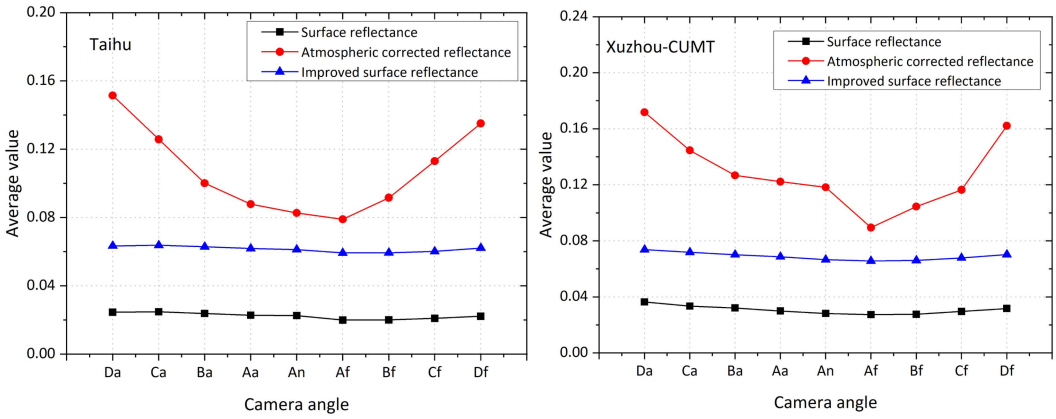

Figure 3. Comparison of MISR surface reflectance, atmospheric corrected reflectance and improved surface reflectance in the blue band (This is multi-year averaged sample data from two sites, Taihu and Xuzhou-CUMT).

To clarify the trend of the improved surface reflectance, the study conducted a time-series analysis of the MISR surface reflectance and the improved surface reflectance. The improved

MISR surface reflectance is always higher than the previously estimated MISR surface reflectance (Figure 4). The MISR surface reflectance is generally between 0 and 0.05, while the improved surface reflectance values is about 0.05 to 0.1. Overall, the improved surface reflectance was increased.

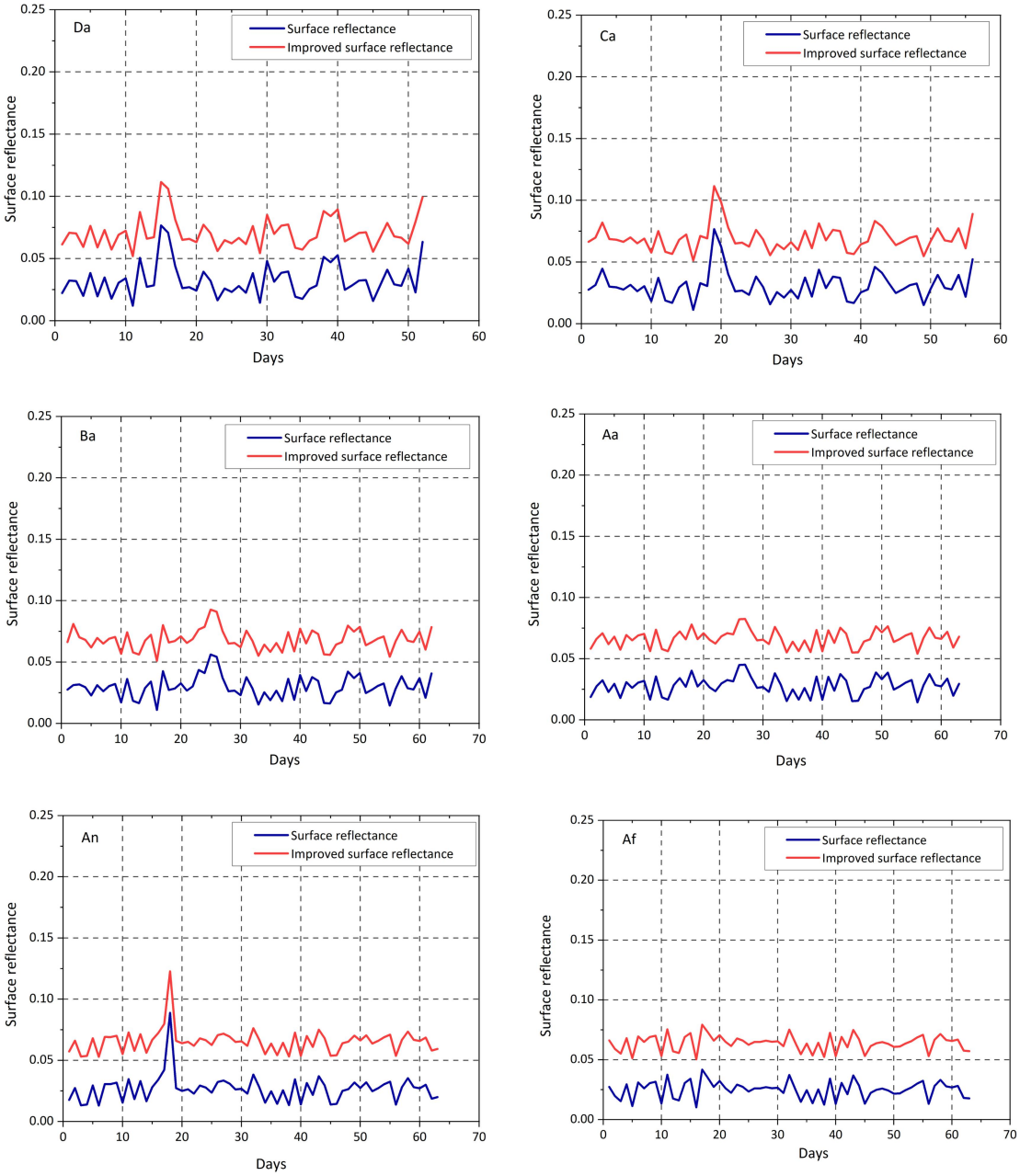

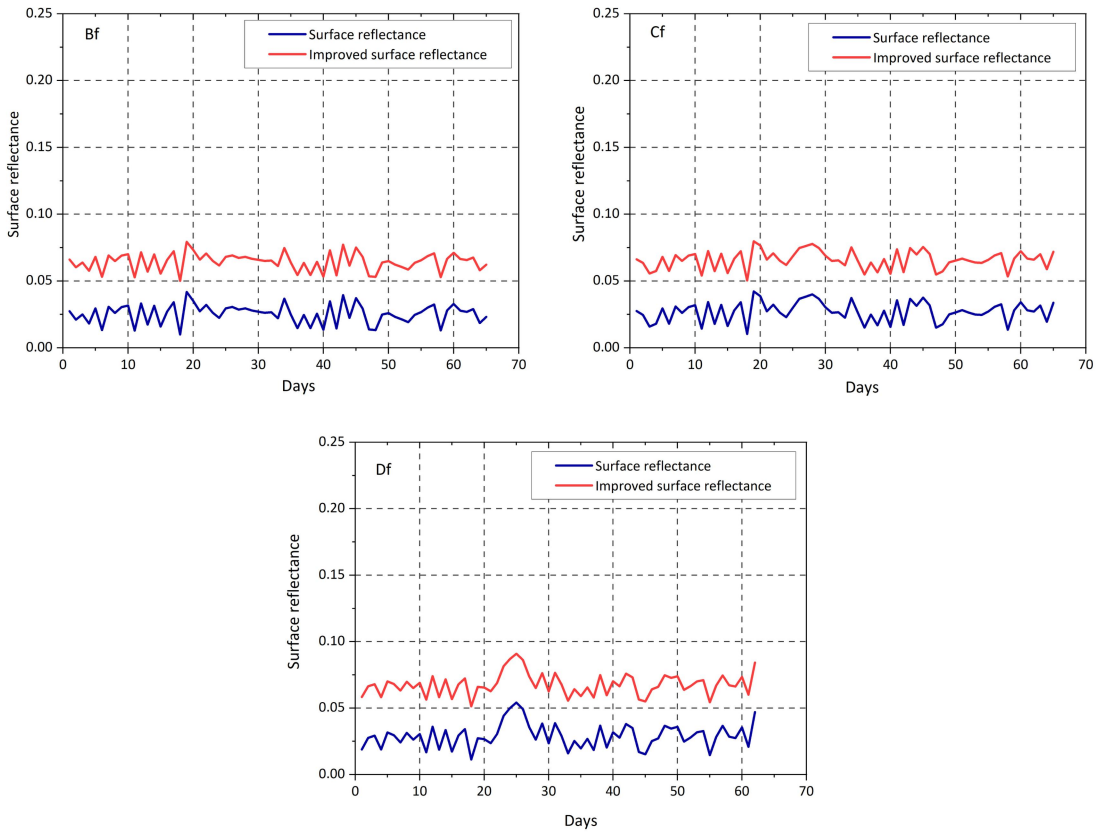

261 **Figure 4.** Time series of surface reflectance in the blue band of the MISR sensor for 9 observation
262 angles (Table S2 lists the time series of the 9 angles from front to back)

263 **4.2 Improved MISR AOD retrieval results**

264 Three years of MISR AOD results were obtained using improved surface reflectance retrieval.
265 This study gives the results of the retrieval of the MISR sensor on June 12, 2018 for nine camera
266 observation angles (Figure 5). From the spatial distribution of AOD, it can be seen that the
267 retrieval results in the study area do not exceed 1. The overall spatial distribution trend is
268 generally consistent with the pre-improvement results (Chen et al., 2021), but there are differences
269 in the magnitude of the values. The values in the northeast and south range from 0.5 to 1,
270 indicating poor air quality in these areas. The AOD values retrieved from 5 camera observation
271 angles Ba, Aa, An, Af, and Bf are in the approximate range of 0.25-0.5. In the central region, most

of the AOD values from the 4 camera observation angles Da, Ca, Cf and Df are in the range of 0-0.25. The data show that the air quality in the central region is generally good, and the air pollution level is light in some areas. The higher AOD in southern Shandong and northern Jiangsu may be related to the increased of local aerosol emissions caused by human activities.

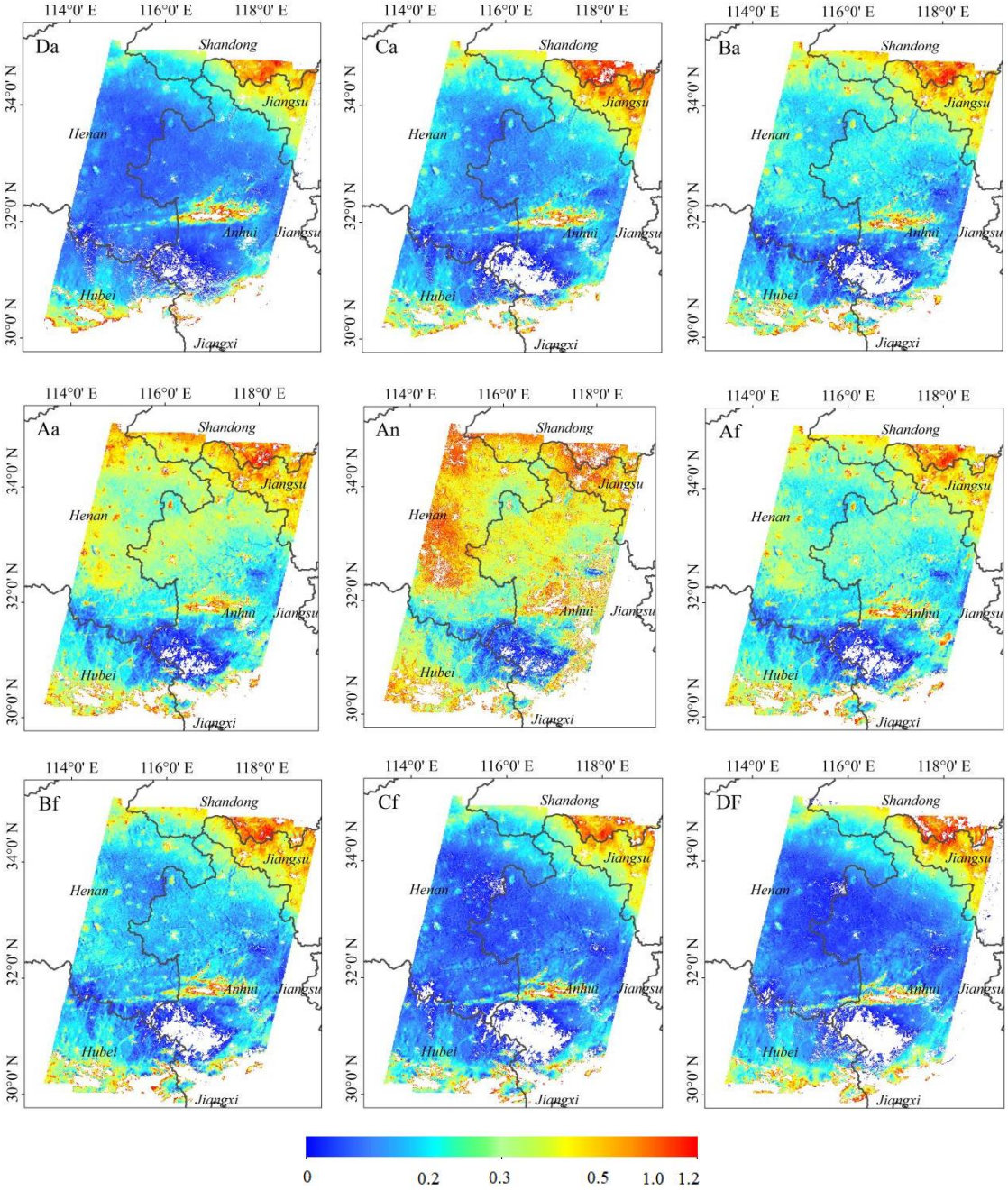

Figure 5. June 12, 2018 Improved MISR AOD retrieval results at 550 nm

The improved MISR AOD spatial distribution results were then validated by comparing them with the MODIS AOD product. The MODIS AOD product has a resolution of 3km. The trends in the spatial distribution of MODIS AOD products are consistent with the improved MISR AOD (Figure 6). However, the MODIS AOD product has more missing data, and the AOD obtained by using the improved algorithm for retrieval can avoid missing data. In addition, the AOD retrieval with the improved algorithm has a higher resolution compared to the image quality of the MISR AOD product.

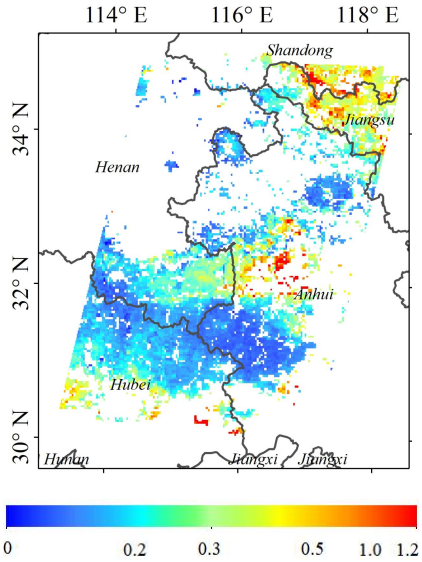

Figure 6. MODIS AOD 550nm product spatial distribution on June 12, 2018

4.3 Verification of improved MISR AOD

There are many AERONET sites in the Yangtze River Delta region, but currently only two sites, Taihu and Xuzhou-CUMT, are able to provide continuous data, and the other sites acquire data on limited time scales. Therefore, we selected the Taihu and Xuzhou-CUMT sites with more data for verification. To validate the retrieved MISR AODs, we selected valid AOD records in the 550nm band within a 30-minute interval between the AERONET ground observation site and the Terra satellite. The MISR sensor 9 camera views take about 7 minutes to be able to observe the

same geographic location at relatively short intervals. Therefore, we used the AERONET AOD averages as approximate truth values and compared them with the retrieved MISR AODs to validate and minimize errors due to time lag. Spatially, we selected the image elements observed by the MISR sensor from nine angles and compared them with the corresponding positional AERONET observations. Since the sun photometer did not have a wavelength of 550nm corresponding to the retrieval results, the AOD at 550nm was calculated by applying Angstrom (Eq. 13).

$$\tau(\lambda) = \beta\lambda^{-\alpha} \tag{13}$$

In the formula, $\tau(\lambda)$ is the AOD at wavelength λ, β is the concentration of aerosols throughout the atmosphere, and α is the wavelength index of Angstrom.

In this study, four parameters, correlation coefficient (R), root mean square error (RMSE), p-value and relative mean bias (RMB), will be used to assess the accuracy of the remotely sensed AOD dataset. The specific calculation principles for the three parameters R, RMSE and RMB are shown in Eq. 14-16. The validation results of AOD dataset of Taihu and Xuzhou-CUMT sites during 2016-2018 after improvement in this study are shown in Figure 7 and Figure 8.

Generally, the scatter plots are distributed above and below the 1:1 line. R is a parameter characterising the correlation between the remote sensing retrieval results and the ground retrieval results. R reached 0.89 for the Taihu site and 0.85 for the Xuzhou-CUMT site. RMSE is a parameter characterising the absolute error of the remote sensing retrieval results, and the minimum RMSE is 0.21 for the Taihu site. The minimum RMSE is 0.20 for the Xuzhou-CUMT site. RMB is a parameter used to describe the relative error of remote sensing retrieval results, and the minimum RMB is 0.52 for the Taihu site and 0.32 for the Xuzhou-CUMT site. Overall, the

retrieval results at angle An are optimal after algorithm improvements (Taihu: R=0.84, RMB=0.52; Xuzhou-CUMT: R=0.85, RMB=0.47). By comparing the results with the pre-improvement AOD validation, the improved AOD retrieval accuracy has been significantly improved (Table 1). In Table 1, R is the correlation between the AOD retrieval results and AERONET AOD before improvement. RMB is the relative deviation between the AOD retrieval by the pre-improvement algorithm and AERONET AOD. Improved R is the correlation between the improved AOD retrieval results and AERONET AOD. Improved RMB is the relative deviation between the AOD retrieved with the improved algorithm and AERONET AOD.

$$R = \frac{\sum_{i=1}^{N}(A_i - \overline{A})(A_i^{'} - \overline{A^{'}})}{\sqrt{\sum_{i=1}^{N}(A_i - \overline{A})^2 \sum_{i=1}^{N}(A_i^{'} - \overline{A^{'}})^2}} \tag{14}$$

$$RMSE = \sqrt{\sum_{i=1}^{N}(A_i - A_i^{'})^2 / N} \tag{15}$$

$$RMB = \sum_{i=1}^{N}(A_i - A_i^{'}) / N \tag{16}$$

where A_i is the retrieve MISR AOD, $A_i^{'}$ is the corresponding AERONET AOD, $\overline{A}$ and $\overline{A^{'}}$ are the mean values of the retrieve MISR AOD and AERONET AOD, respectively. N is the number of valid matching results for AERONET AOD and MISR AOD.

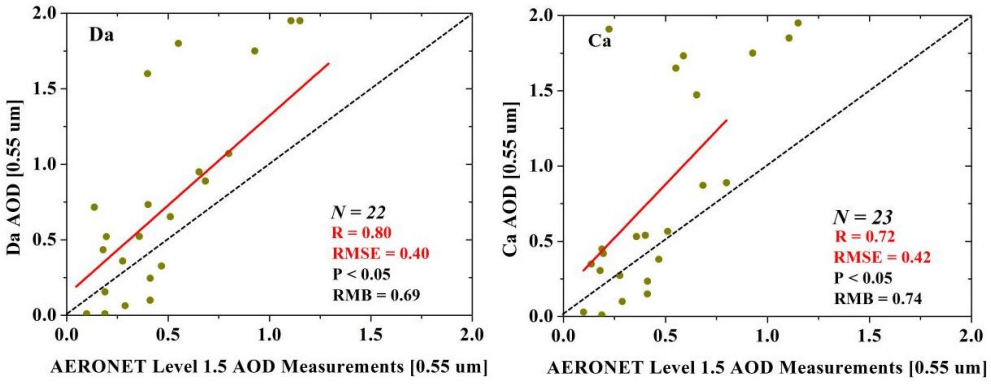

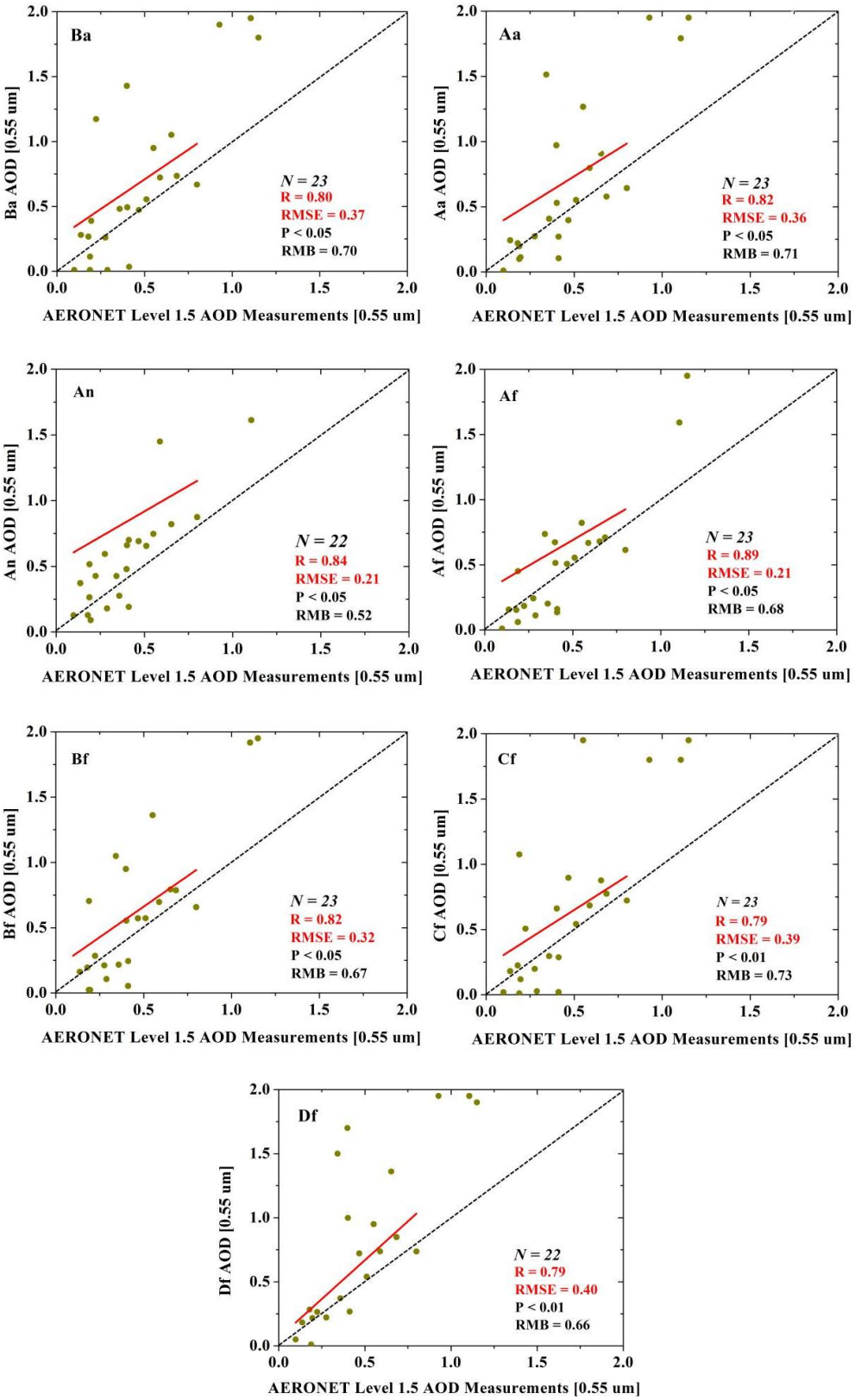

328 **Figure 7.** Comparison between improved MISR AOD and AERONET AOD at Taihu site (N is

329 the number of verification points, red line represents a linear fitting line)

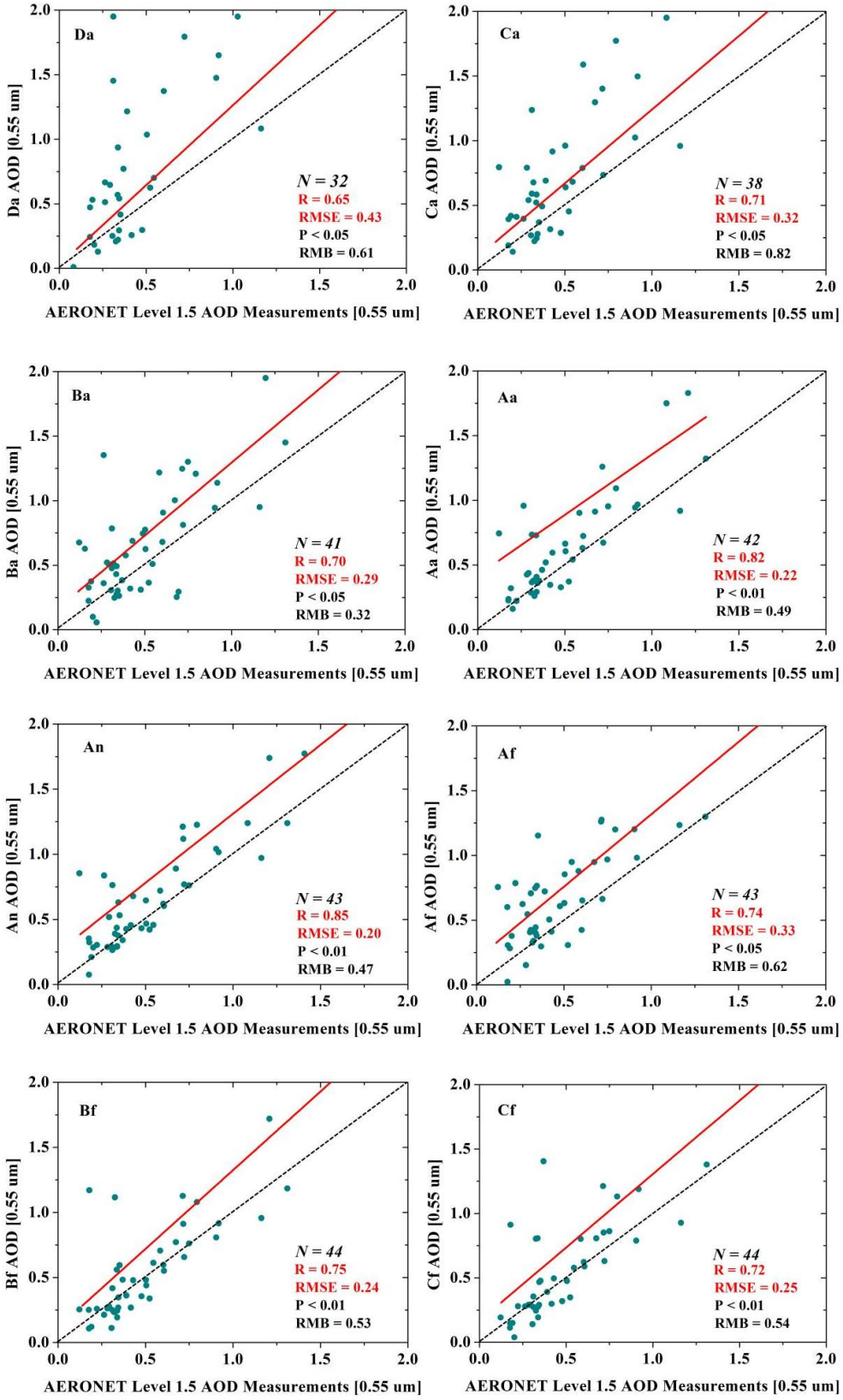
Da
N = 32
R = 0.65
RMSE = 0.43
P < 0.05
RMB = 0.61
Da AOD [0.55 um]
AERONET Level 1.5 AOD Measurements [0.55 um]
Ca
N = 38
R = 0.71
RMSE = 0.32
P < 0.05
RMB = 0.82
Ca AOD [0.55 um]
AERONET Level 1.5 AOD Measurements [0.55 um]
Ba
N = 41
R = 0.70
RMSE = 0.29
P < 0.05
RMB = 0.32
Ba AOD [0.55 um]
AERONET Level 1.5 AOD Measurements [0.55 um]
Aa
N = 42
R = 0.82
RMSE = 0.22
P < 0.01
RMB = 0.49
Aa AOD [0.55 um]
AERONET Level 1.5 AOD Measurements [0.55 um]
An
N = 43
R = 0.85
RMSE = 0.20
P < 0.01
RMB = 0.47
An AOD [0.55 um]
AERONET Level 1.5 AOD Measurements [0.55 um]
Af
N = 43
R = 0.74
RMSE = 0.33
P < 0.05
RMB = 0.62
Af AOD [0.55 um]
AERONET Level 1.5 AOD Measurements [0.55 um]
Bf
N = 44
R = 0.75
RMSE = 0.24
P < 0.01
RMB = 0.53
Bf AOD [0.55 um]
AERONET Level 1.5 AOD Measurements [0.55 um]
Cf
N = 44
R = 0.72
RMSE = 0.25
P < 0.01
RMB = 0.54
Cf AOD [0.55 um]
AERONET Level 1.5 AOD Measurements [0.55 um]

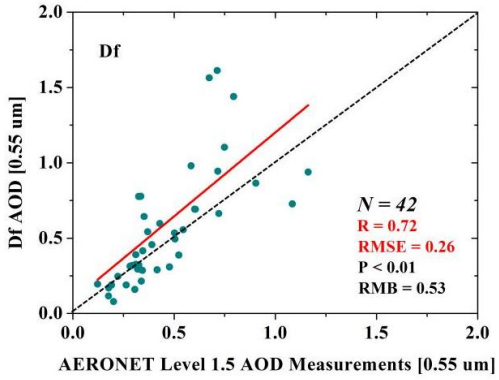

330 **Figure 8.** Comparison between improved MISR AOD and AERONET AOD at Xuzhou-CUMT

331 site (N is the number of verification points, red line represents a linear fitting line)

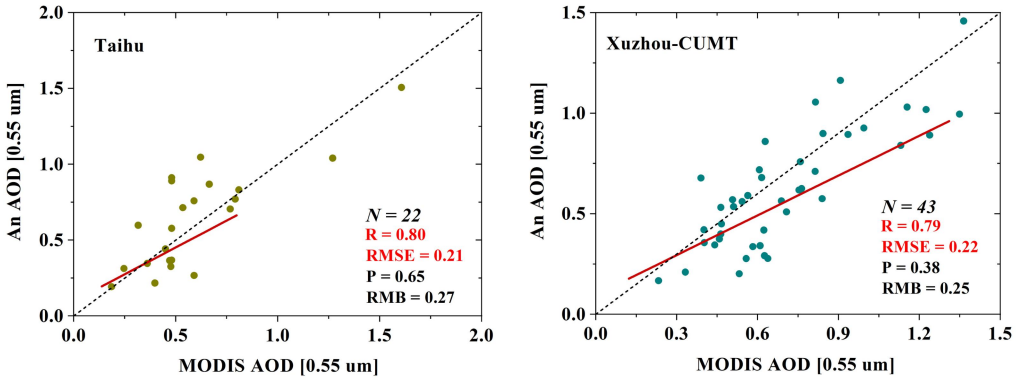

332

333 **Figure 9.** Comparison of validation of retrieved AOD with MODIS AOD product

334 **Table 1.** Precision comparison of MISR AOD and AERONET AOD before

335 and after improvement

Site	Angle	R	RMB	Improved R	Improved RMB
Taihu	Da	0.77	1.08	0.80	0.69
	Ca	0.70	1.00	0.72	0.74
	Ba	0.77	0.61	0.80	0.70
	Aa	0.81	0.68	0.82	0.71
	An	0.45	1.22	0.84	0.52
	Af	0.72	0.87	0.89	0.68
	Bf	0.72	0.60	0.82	0.67
	Cf	0.57	0.65	0.79	0.73
	Df	0.77	0.47	0.79	0.66
Xuzhou-	Da	0.45	1.58	0.65	0.61

CUMT	Ca	0.59	0.96	0.71	0.82
	Ba	0.67	0.78	0.70	0.32
	Aa	0.73	0.78	0.82	0.49
	An	0.75	0.85	0.85	0.47
	Af	0.72	0.63	0.74	0.62
	Bf	0.62	0.65	0.75	0.53
	Cf	0.68	0.66	0.72	0.54
	Df	0.67	0.65	0.72	0.53

Comparing the validation results of the MODIS AOD product with those of the observation sites (Taihu: R=0.59, RMSE=0.19, P<0.05, RMB=0.52; Xuzhou-CUMT: R=0.71, RMSE=0.25, P<0.05, RMB=0.44) (Chen et al., 2021), we found that the Taihu and Xuzhou-CUMT sites have high correlation between the improved MISR AOD and MODIS AOD products. The smaller observation angle of the improved MISR AOD, the closer the error is to the MODIS AOD product. The observation angle of MISR An is the same as that of MODIS. Therefore, we selected two sites for validation at the An observation angle and MODIS AOD product (Figure 9). The results show that the An AOD retrieval by the improved algorithm correlates well with the MODIS AOD product. The position errors of the two image elements are close to each other. The RMSE of the Xuzhou-CUMT site is slightly higher than that of Taihu site, and the RMB of Taihu site is slightly higher than that of the Xuzhou-CUMT site.

5. Conclusion

In this study, we first explored the problems of estimating surface reflectance in our previous study. We obtained an error correction model for surface reflectance by using a linear fit of the MISR surface reflectance and a new estimate of the MISR surface reflectance. The improved MISR surface reflectance was obtained through the error correction model. We then retrieved a

new AOD product using the improved surface reflectance and a lookup table constructed from the 6S model. Two AERONET ground observation sites with longer time series were used to validate the AOD obtained by satellites.

(1) Overall, the improved AOD and its spatial distribution trends are consistent with our previous results. The AOD estimated by improved method exhibited higher accuracy and a high degree of agreement with the AERONET ground-based observational AOD. Overall, the retrieval results at angle An are optimal after algorithm improvements (Taihu: R=0.84, RMB=0.52; Xuzhou-CUMT: R=0.85, RMB=0.47). The improvements at the Xuzhou-CUMT site are more pronounced compared to the Taihu site.

(2) More importantly, the optimal AOD obtained in this study has fewer missing pixels and finer spatial resolution than the MODIS AOD product. Through the validation with MODIS AOD products, the AOD of An optimal angle obtained by the improved algorithm is highly correlated with MODIS AOD products.

(3) In future, more aerosol models that conform to the actual situation in the study area can be constructed using the AERONET ground observation data and introduced into the MISR AOD retrieval algorithm to further improve the accuracy of the AOD retrieval results. In this study, the AERONET AOD was used as the true value and as an input for the AOD parameter in the 6S model for atmospheric correction of MISR and MODIS images. We then obtained a surface reflectivity error correction model to retrieve AOD for the entire region. It should be emphasized that the more AERONET sites used to train the corrected model, the more accurate AOD retrieved may be obtained by this method. However, the data from the AERONET ground observation sites were limited. In future, the study area can be expanded on a large scale and for a longer time

series.

Acknowledgement

This study was supported by the National Natural Science Foundation of China Innovation Research Group Project (42021004), Jiangsu Funding Program for Excellent Postdoctoral Talent (2023ZB482), the Natural Science Foundation of Jiangsu Province of China (BK20220455), and the National Science Foundation of China (42201028).

Competing interests

The contact author has declared that none of the authors has any competing interests.

383 **Reference**

384 Berhane, S. A.; Bu, L. Aerosol-Cloud Interaction with Summer Precipitation over Major Cities in
385 Eritrea[J]. Remote Sens-basel, 2021, 13(4):21.

386 Chen, L.; Wang, R.; Han J. Influence of observation angle change on satellite retrieval of aerosol
387 optical depth[J]. Tellus B, 2021, 73.

388 Chen, L.; Fei, Y.; Wang, R. Retrieval of high temporal resolution aerosol optical depth using the
389 GOCI remote sensing data[J]. Remote Sens-basel. 2021, 13:2376.

390 Chen, L.; Wang, R.; Wei, G. A surface reflectance correction model to improve the retrieval of
391 MISR aerosol optical depth supported by MODIS data[J]. Adv Space Res, 2021,
392 67(2):858-867.

393 Dao, Y.; Gong, W. Observed holiday aerosol reduction and temperature cooling over East Asia[J].
394 J Geophys Res-atmos, 2014.

395 Daniel, R.; Steven, S.; Robert, W.; Leo, D. Climate Effects of Aerosol-Cloud Interactions[J].
396 Science, 2014, 343, 379-380.

397 Dehghani, M.; Saeedi, A. A.; Zamanian, Z. A study of the relationship between indoor and outdoor
398 particle concentrations in Hafez hospital in Shiraz[J]. Phys.Rev.C, 2012.

399 Dong, W.; Tao, M.; Xu, X.; Wang, J.; Wang, Y.; Wang, L.; Song, Y.; Fan, M.; Chen, L. Satellite
400 Aerosol Retrieval From Multiangle Polarimetric Measurements: Information Content and
401 Uncertainty Analysis," IEEE Trans. Geosci. Remote Sens. 2023, 61, 1-13.

402 Dubovik, O.; Li.; Mishchenko M. I. Polarimetric remote sensing of atmospheric aerosols:
403 Instruments, methodologies, results, and perspectives[J]. Pergamon, 2019, 474-511.

404 Deuzé, J. L.; Bréon, F. M.; Devaux, C.; Goloub, P.; Herman, M.; Lafrance, B.; Maignan, F.;

405 Marchand, A.; Nadal, F.; Perry, G.; Tanré, D. Remote sensing of aerosols over land surfaces
406 from POLDER-ADEOS-1 polarized measurements. J Geophys Res-atmos, 2001, 106(D5):
407 4913-4926.
408 Giles, D. M.; Sinyuk, A.; Sorokin, M. G. Advancements in the Aerosol Robotic Network
409 (AERONET) Version 3 database-automated near-real-time quality control algorithm with
410 improved cloud screening for Sun photometer aerosol optical depth (AOD) measurements[J].
411 Copernicus GmbH, 2019, 12(1), 169-209.
412 Gupta, P.; Levy, R. C.; Mattoo, S. A surface reflectance scheme for retrieving aerosol optical depth
413 over urban surfaces in MODIS dark target retrieval algorithm[J]. Atmos Meas Tech, 2016,
414 9(7): 3293-3308.
415 Hatzianastassiou, N. The direct effect of aerosols on the radiation budget and climate of the
416 Earth-atmosphere system: its variability in space and time. EGU General Assembly
417 Conference Abstracts EGU General Assembly Conference Abstracts, 2009.
418 Holben, B. N.; Tanré, D.; Smirnov, A. An emerging ground-based aerosol climatology: Aerosol
419 optical depth from AERONET[J]. J Geophys Res, 2001, 106, 12067-12097.
420 Huang, X.; Ding, A. Aerosol as a critical factor causing forecast biases of air temperature in global
421 numerical weather prediction models[J]. Science Bulletin, 2021.
422 Hsu, N. C.; Tsay, S. C.; King, M. D. Aerosol properties over bright-reflecting source regions[J].
423 IEEE Trans. Geosci. Remote Sens, 2004, 42(3):557- 569.
424 Kaufman, Yoram J. The MODIS 2.1-um channel--correlation with visible reflectance for use in
425 remote sensing of aerosol.[J]. IEEE T Geosci Remote, 1997, 35, 1286-1298.
426 Kokhanovsky, A. A.; Curier, R. L.; Leeuw, G. D.; Grey, W. M. F. The intercomparison of AATSR

427 dual-view aerosol optical thickness retrievals with results from various algorithms and
428 instruments. Int. J. Remote Sens. 2009, 30 (17): 4525-4537.
429 Lee, S. S.; Donner L. J.; Penner J. E. Thunderstorm and stratocumulus: How does their contrasting
430 morphology affect their interactions with aerosols?[J]. Atmos. Chem. Phys. 2010, 10(2),
431 6819-6837.
432 Li, E.; Zhang, Z.; Tan, Y. A Novel Cloud Detection Algorithm Based on Simplified Radiative
433 Transfer Model for Aerosol Retrievals: Preliminary Result on Himawari-8 Over Eastern
434 China[J]. IEEE T Geosci Remote, 2020, 59(3):1-12.
435 Li, Y.; Xue, Y.; Guang, J. Ground-Level PM2.5 Concentration Estimation from Satellite Data in
436 the Beijing Area Using a Specific Particle Swarm Extinction Mass Conversion Algorithm[J].
437 Remote Sens-basel, 2018, 10(12), 1906.
438 Lu, S.; Xue, Y.; Yang, X.-H.; Leys, J.; Guang, J.; Che, Y.-H.; Fan, C.; Xie, Y.Q.; Li, Y. Joint
439 Retrieval of Aerosol Optical Depth and Surface Reflflectance Over Land Using
440 Geostationary Satellite Data. IEEE Trans. Geosci. Remote Sens. 2019, 57, 1489–1501.
441 Mironova, I. A. Aerosols over continental Portugal (1978-1993): their sources and an impact on
442 the regional climate[J]. Atmos. Chem. Phys. 2015, 15(11):6407-6418.
443 Remer, L. A; Tanré, D.; Kaufman, Y. J. Algorithm for remote sensing of tropospheric aerosol from
444 MODIS: Collection 005[J]. 2009.
445 Samset, B. H.; Sand, M.; Smith, C. J. Climate Impacts From a Removal of Anthropogenic Aerosol
446 Emissions[J]. Geophys Res Lett, 2018, 45(2).
447 Sun, E.; Fu, C.; Yu, W. Variation and Driving Factor of Aerosol Optical Depth over the South
448 China Sea from 1980 to 2020[J]. Atmosphere, 2022, 13, 372.

449 Sundstrom, A. M.; Kolmonen, P.; Sogacheva, L.; Leeuw, G. D. Aerosol retrieval over China with
450 the AATSR dual view algorithm. Remote Sens. Environ. 2012, 116 (1): 189-198.
451 Xie, Y.; Xue, Y.; Jie, G. Deriving a Global and Hourly Data Set of Aerosol Optical Depth Over
452 Land Using Data From Four Geostationary Satellites: GOES-16, MSG-1, MSG-4, and
453 Himawari-8[J].IEEE T Geosci Remote, 2019, 99:1-12.
454 Zhang, Y.; Li, Z.; Liu, Z. Retrieval of aerosol fine-mode fraction over China from satellite
455 multiangle polarized observations: validation and comparison[J]. Atmos Meas Tech, 2021, 2,
456 1655-1672.